ChemPubSoc Europe

DOI: 10.1002/chem.201702727

CHEMISTRY
A European Journal
Communication

■ Ru Complexes |*Hot Paper*|

Metalloradical Reactivity of Ru^{I} and Ru^{0} Stabilized by an Indole-Based Tripodal Tetraphosphine Ligand

Fenna F. van de Watering, Jarl Ivar van der Vlugt, Wojciech I. Dzik,* Bas de Bruin,* and Joost N. H. Reek*[a]

Abstract: The tripodal, tetradentate tris(1-(diphenylphosphanyl)-3-methyl-1*H*-indol-2-yl)phosphane PP_3-ligand **1** stabilizes Ru in the Ru^{II}, Ru^{I}, and Ru^{0} oxidation states. The octahedral $[(PP_3)Ru^{II}(Cl)_2]$ (**2**), distorted trigonal bipyramidal $[(PP_3)Ru^{I}(Cl)]$ (**3**), and trigonal bipyramidal $[(PP_3)Ru^{0}(N_2)]$ (**4**) complexes were isolated and characterized by single-crystal X-ray diffraction, NMR, EPR, IR, and ESI-MS. Both open-shell metalloradical Ru^{I} complex **3** and the closed-shell Ru^{0} complex **4** undergo facile (net) abstraction of a Cl atom from dichloromethane, resulting in formation of the corresponding Ru^{II} and Ru^{I} complexes **2** and **3**, respectively.

Metals of the 4d and 5d row of the periodic table, particularly late transition metals in low oxidation states, strongly prefer closed-shell 16 or 18 valence electron configurations. As a result, open-shell complexes of these metals are rare, and have a strong tendency to convert into closed-shell products.[1] Ru^{I} metalloradical complexes are particularly rare[2] and only two types of Ru^{I} complexes have been successfully isolated thus far. Peters and co-workers reported a five-coordinate 17-electron $[Ru^{I}N_2(SiP^{iPr}_3)]$ complex supported by an anionic tripodal tetradentate $(SiP^{iPr}_3)^-$ ligand $(SiP^{iPr}_3 = (2\text{-}i\text{Pr}_2\text{PC}_6\text{H}_4)_3\text{Si})$. Besides Ru^{I}, this platform also stabilizes complexes in oxidation states ranging from Ru^{0} to Ru^{III}.[3] Interestingly, the Ru^{I} complex was shown to catalyze coupling of aryl azides to azoarenes.[4] Recently, the group of Grützmacher reported the remarkable 4-coordinate 15-electron complex $[Ru^{I}(tropPPh_2)_2]BF_4$ featuring two bidentate $tropPPh_2$ ligands (trop = 5*H*-dibenzo[*a*,*d*]cyclohepten-5-yl)). Besides Ru^{I}, this ligand scaffold stabilizes ruthenium complexes in oxidation states ranging from Ru^{0} to Ru^{II}.[5] No further reactivity with this complex has been reported to date.

Inspired by these intriguing examples, we wondered whether stable metalloradical Ru^{I} complexes could be accessed in a rigid tripodal PP_3 ligand environment for subsequent reactivity evaluation. The above-mentioned Ru^{I} complexes feature either a strongly σ-donating anionic tripodal $(SiP^{iPr}_3)^-$ ligand or two neutral π-accepting bidentate $(tropPPh_2)$ ligands. Hence, we surmised that the use of a tripodal tetradentate ligand featuring both σ-donor and π-accepting phosphorus groups could allow for isolation and reactivity studies of well-defined Ru^{I} metalloradicals. We turned our attention to the tripodal, tetradentate tris(1-(diphenylphosphanyl)-3-methyl-1*H*-indol-2-yl)phosphane ligand (**1**)[6,7] (Figure 1), which we previously used to stabilize the metalloradical rhodium complex $[Rh^{II}(\mathbf{1})Cl]PF_6$.[6] We further wondered whether the corresponding ruthenium(0) complex could also be accessible and if these low-valent species would display interesting reactivity.

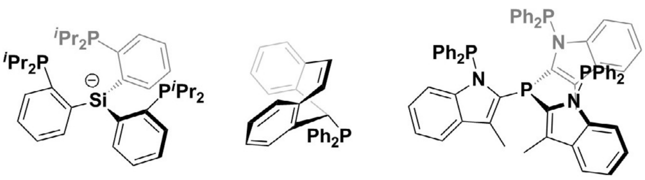

Figure 1. Ligand systems capable of stabilizing isolable Ru^{I} species.

First, we aimed at the synthesis of the Ru^{II} complex with ligand **1**, as this species could allow entry to the desired low-valent ruthenium species by subsequent selective reduction. The desired complex $[Ru(\mathbf{1})(Cl)_2]$ (**2**) was readily prepared by reacting stoichiometric amounts of **1** and $[Ru(Cl)_2(C_6H_6)]_2$ in refluxing THF in good yield (Scheme 1).

The ^{31}P NMR spectrum of complex **2** displays a triplet of doublets ($\delta = 101.0$ ppm, $J_{P\text{-}P} = 26.4$, 25.5 Hz), an apparent triplet ($\delta = 77.8$ ppm, $J_{P\text{-}P} = 26.5$ Hz), and a triplet of doublets ($\delta = 48.5$ ppm, $J_{P\text{-}P} = 27.9$, 26.9 Hz) with the integral ratio 1:2:1. The presence of three different phosphorus NMR signals points to a geometry in which two equatorial aminophosphine donors

[a] Dr. F. F. van de Watering, Dr. Ir. J. I. van der Vlugt, Dr. W. I. Dzik, Prof. Dr. B. de Bruin, Prof. Dr. J. N. H. Reek
Homogeneous, Supramolecular and Bio-Inspired Catalysis
Van't Hoff Institute for Molecular Sciences
University of Amsterdam
Science Park 904
1098 XH Amsterdam (The Netherlands)
E-mail: wdzik@wp.pl
B.debruin@uva.nl
J.N.H.Reek@uva.nl

Supporting information and the ORCID identification number(s) for the author(s) of this article can be found under https://doi.org/10.1002/chem.201702727.

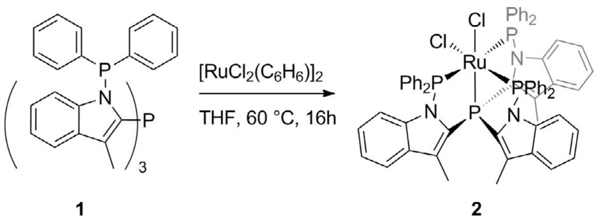

Scheme 1. Synthesis of [Ru(**1**)(Cl)$_2$] (**2**).

are equivalent ($\delta = 77.8$ ppm), whereas the third side-arm donor P3 ($\delta = 101.0$ ppm) experiences a different coordination environment. The pivotal, axial phosphine P4 is assigned to the signal at $\delta = 48.5$ ppm. Ru^{II} complexes with tripodal tetraphosphine ligands often display five-coordination with either square pyramidal or trigonal bipyramidal geometries around the metal center,[8] however in case of complex **2**, an octahedral geometry could not be excluded. Single crystals of **2**, suitable for single crystal X-ray diffraction, were obtained by layering a dichloromethane solution with pentane. The molecular structure (Figure 2) reveals a distorted octahedral geometry, with ∡P1–Ru1–P2 of 160.04(3)° (See the Supporting Information, Table S1) for the two mutually *trans* aminophosphines in the equatorial plane. The P donors oriented *trans* to the chlorido ligands have shorter Ru–P distances (Ru1–P3 (2.2671(9) Å; Ru1–P4 (2.1932(9) Å) compared to the mutually *trans* P donors (Ru1–P1 (2.3727(9) Å; Ru1–P2 (2.3189(9) Å).[9]

To explore the capability of **1** to stabilize low oxidation states of ruthenium, we attempted to determine the Ru^{II}/Ru^{I} and Ru^{I}/Ru^{0} reduction potentials of **2**. The cyclic voltammogram of **2** in dichloromethane did not show any reduction wave within the solvent window ($E_{min} = -2.5$ vs. Fc/Fc$^+$), and the poor solubility of **2** in THF, DMF, acetonitrile, or toluene prevented determination of the reduction potentials of **2** below -2.5 V. Thus, reduction of complex **2** to the desired complex [Ru(**1**)Cl] (**3**) requires a stronger reducing agent than the previously reported Ru^{I} complexes [-1.24 V (Ru^{II}/Ru^{I}) and -2.14 V (Ru^{I}/Ru^{0}) for the SiP$^{iPr}_3$ system in THF; $+0.4$ V (Ru^{II}/Ru^{I}) and -0.3 V (Ru^{I}/Ru^{0}) for the tropPPh$_2$ complex]. Therefore, we used KC$_8$ to access the desired Ru^{I} and Ru^{0} species chemically (Scheme 2).

The addition of one molar equivalent of KC$_8$ to a yellow suspension of **2** in THF resulted in a brown solution. The product formed proved to be NMR silent, suggestive of formation of a paramagnetic Ru^{I} species formed by one-electron reduction. X-band EPR spectroscopy confirmed the presence of the metalloradical species [Ru(**1**)Cl] (**3**). The EPR spectrum reveals a rhombic (albeit almost axial) *g*-tensor, characteristic of an $S = {}^1/_2$ system (Figure 3). Hyperfine coupling interactions (HFIs) with two P atoms are resolved, in line with previous observations for tripodal tetradentate phosphine Ru^{I} complexes.[2c,e,3]

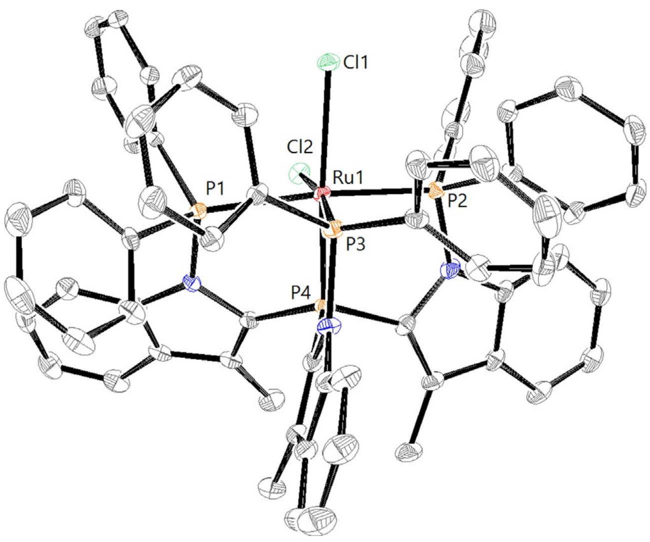

Figure 2. X-ray crystal structure of **2** (CCDC 1555408). Thermal ellipsoids are set at 50% probability. Solvent molecules and hydrogen atoms have been omitted for clarity.

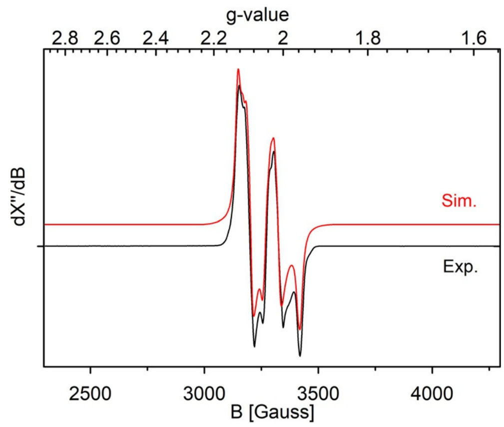

Figure 3. Experimental (black) and simulated (red) X-band EPR spectrum of **3** measured in frozen THF ([Bu$_4$N][PF$_6$] was added to obtain an improved glass). Experimental conditions: Temperature 20 K, microwave power 0.063 mW, field modulation amplitude 4 G, microwave frequency 9.3646 GHz. The simulated spectrum was obtained with the parameters shown in Table S2.

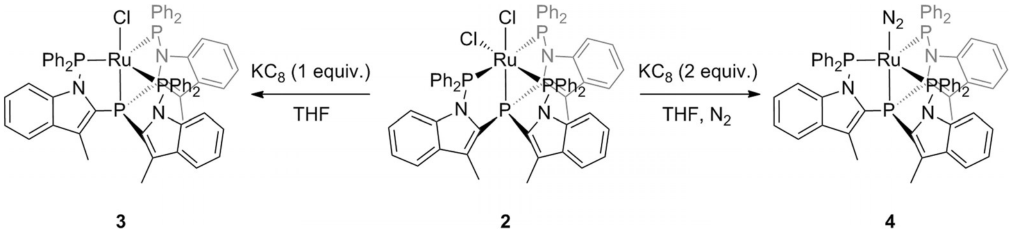

Scheme 2. Reactivity of **2** with 1 or 2 equiv KC$_8$ to form **3** or **4**, respectively.

These results are in agreement with a geometry that is distorted from a trigonal bipyramidal toward a (distorted) square pyramidal Ru^{I} coordination geometry. Preference for such a Jahn–Teller distorted trigonal bipyramidal geometry has also been observed for other d^7 transition metal complexes.[10]

Simulation of the experimental EPR spectrum revealed the parameters shown in Table S2 (see also the captions of Figures 3 and 5). The geometry of **3** was optimized with DFT (Turbomole, BP86, def2-TZVP), and the EPR parameters were computed with Orca and ADF. The DFT-computed EPR parameters (Table S2) are in qualitative agreement with the experimental data. The computations reveal a mainly metal-centered spin density distribution, as evident from the singly occupied molecular orbital (SOMO) and spin density plots of **3** (Figure 4).

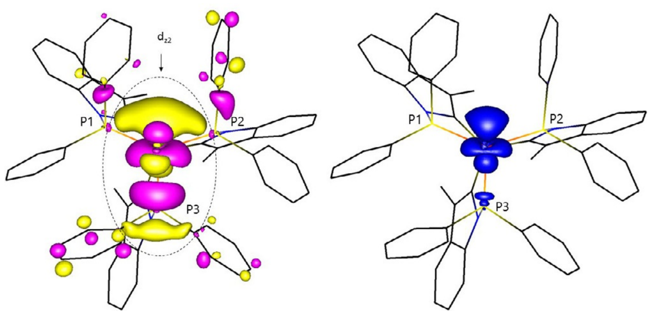

Figure 4. Singly occupied molecular orbital (SOMO; left) and spin density plot (right) of **3** (top view).

The SOMO of the metalloradical complex (spin population at Ru = 62%) is essentially the Ru d_{z^2} orbital pointing in the direction of the apical P donor (P3) of the distorted trigonal bipyramid (Figure 4, left). As a result, the spin population of the axial P donor (P3) is significant (ca. 12%; Figure 4, right), thus explaining the observed large HFIs with this donor atom. The two P donors in the distorted equatorial plane bind rather asymmetrically, leading to a larger spin population at one (8%, P2) compared to the other (5%, P1) P donor. The spin population at the connecting P donor *trans* to the chlorido ligand is small and negative (−0.8%, P4). The resolved HFIs in the experimental X-band EPR spectrum are thus well-explained by the electronic structure of **3**. The *g*-anisotropy of complex **3** is quite small for a metalloradical complex, but this is fully understandable considering the large energy separation (Turbomole, BP86, def2-TZVP) between the d_{z^2}-dominated SOMO and the filled d_{xz} and d_{yz}-dominated MOs (1.4 eV and 1.6 eV, respectively).[1d]

The small *g*-anisotropy of **3** allows for recording the isotropic EPR spectrum in THF solution at room temperature (Figure 5). Simulation reveals a g_{iso} value of 2.047 and HFIs with three equivalent P atoms ($A_P^{iso} = 143$ MHz). The measured g_{iso} value is close to the average value of the anisotropic *g*-tensor components ($g_{av} = (g_x + g_y + g_z)/3 = 2.043$). Detection of HFIs with three equivalent P atoms in solution points to rapid positional exchange of the axial and equatorial PPh_2 donors on the EPR timescale. In line with this, the measured A_P^{iso} values measured in solution are close to the averaged values of the resolved anisotropic *A*-tensor components stemming from the PPh_2 donors measured in frozen solution ($A_P^{av} = (A_{P1}^x + A_{P1}^y + A_{P1}^z + A_{P2}^x + A_{P2}^y + A_{P2}^z)/9 = 157$ MHz).

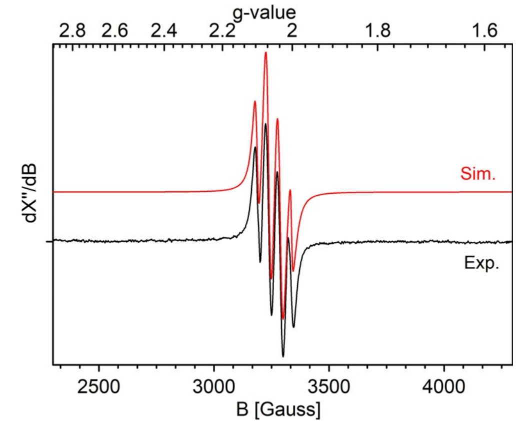

Figure 5. Experimental (black) and simulated (red) X-band EPR spectrum of **3** in isotropic solution (THF). Experimental conditions: Temperature 298 K, microwave power 2.0 mW, field modulation amplitude 4 G, microwave frequency 9.3498 GHz. The simulated spectrum was obtained with $g_{iso} = 2.0465$, $A_P^{iso} = 143$ MHz (3 equivalent P atoms), $W_{iso} = 25$ MHz.

Layering of a THF solution of **3** with pentane resulted in the formation of brown needles suitable for single-crystal X-ray diffraction analysis. The molecular structure (Figure 6) is in good agreement with the EPR data and the DFT-optimized structure. The τ-value of 0.70 confirms a geometry in-between a trigonal bipyramid and a square pyramid.[11] The one-electron reduction of **2** to **3** is accompanied by the loss of one chlorido ligand and shortening of most of the Ru–P bonds (Ru–P1 = 2.2940(12); Ru–P2 = 2.2930(12) Å) and decrease of the ∡P1–Ru–P2 angle to 134.84(5)° (See the Supporting Information, Table S1).

As one-electron chemical reduction of complex **2** led to the selective formation of the stable Ru^{I} complex **3**, we also explored two-electron reduction of complex **2**. Addition of two equivalents of KC_8 to a THF suspension of **2** under N_2 atmos-

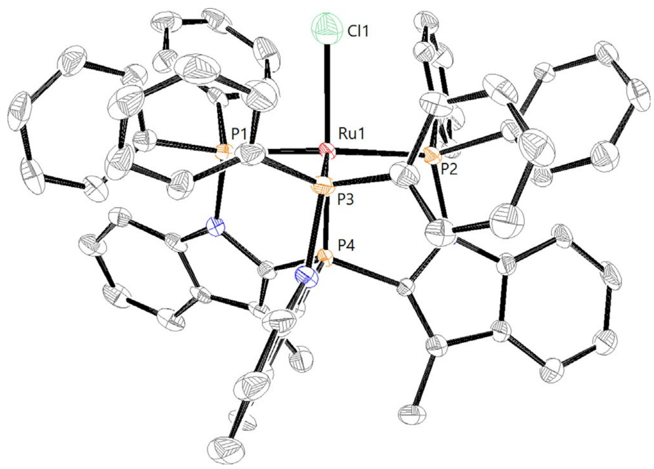

Figure 6. X-ray crystal structure of **3** (CCDC 1555409). Thermal ellipsoids are set at 50% probability. Solvent molecules and hydrogen atoms have been omitted for clarity.

phere led to formation of the Ru^0 dinitrogen complex $[Ru^0(\mathbf{1})(N_2)]$ (**4**). IR spectroscopy reveals the presence of an absorption at $\nu_{N_2} = 2125\ cm^{-1}$, which indicates the formation of a coordinated dinitrogen ligand that is weakly activated.[12] The ^{31}P NMR spectrum shows a doublet and a quartet in a 3:1 ratio, both with a coupling constant $J_{P\text{-}P}$ of 39 Hz. This coupling is in agreement with a C_3-symmetric complex with three equivalent peripheral phosphine atoms that couple with the central P atom in the axial position.

Brick-red colored crystals of **4** suitable for X-ray diffraction were grown by diffusion of pentane into a THF solution of the filtered reaction mixture. The molecular structure confirms formation of complex **4** with dinitrogen coordinated to the ruthenium (Figure 7). Complex **4** has a trigonal bipyramidal geome-

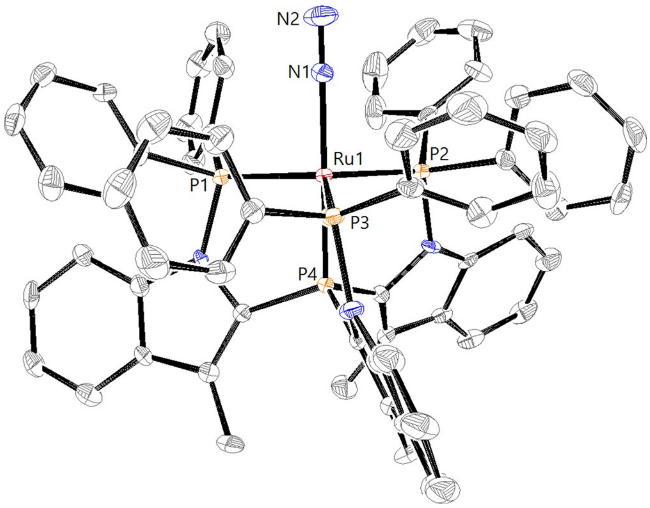

Figure 7. X-ray crystal structure of **4** (CCDC 1555410). Thermal ellipsoids are set at 50 % probability. Solvent molecules and hydrogen atoms have been omitted for clarity.

try ($\tau = 0.93$) with equal Ru–$P_{equatorial}$ bond lengths (Ru–P1 = Ru1 P1 2.2747(12); Ru–P2 = 2.2752(11); Ru–P3 = 2.2774(11)), and ∡P–Ru–P angles that are close to 120°. Additionally, the P4–Ru bond (2.2133(11) Å) *trans* to N_2 is elongated relative to **2** and **3**. This is likely a result of weakening of the π backbonding between Ru and P4 attributable to competition for the same metal orbital with the π-acidic dinitrogen ligand. The general shortening of all Ru–P bonds on progressing from Ru^{II} via Ru^{I} to Ru^0 in complexes **2**, **3**, and **4** is somewhat unexpected, as a lower oxidation state of the metal center is intuitively expected to result in weaker binding of σ-donor ligands. The stronger metal–phosphorus interactions observed instead are likely the result of several contributing effects. Going from an octahedral six-coordinate species (Ru^{II}) to a distorted trigonal bipyramidal (Ru^{I}) and a trigonal bipyramidal (Ru^0) five-coordinate species lowers the steric hindrance between the phosphorus atoms and allows for better overlap of Ru and P orbitals, resulting in shortening of the Ru–P bonds. Another factor that can play a role is that the P1 and P2 phosphorus donor atoms compete strongly for the same metal orbital as they are in a *trans* arrangement in complex **2**. Binding to separate metal orbitals becomes possible upon decreasing the ∡P1–Ru–P2 angle, which is observed in going from **2** (160.04(3)°) to **4** (122.85(4)°), thus explaining the shortening of the Ru–P1 and Ru–P2 bonds. Moreover, the π-acidic character of the aminophosphines P1, P2, and P3 can become dominant over their σ-donating capacities in the electron-rich Ru^0 complex **4**.

With the low oxidation state ruthenium complexes **3** and **4** in hand, we decided to explore their reactivity. Both Roper and Grubbs reported the formation of dichlorido Ru^{II} carbenes upon addition of α,α-dihalide and trihalide compounds to Ru^0 complexes, where both the chloride and the carbene ligands originate from the organohalide.[13] The reaction was proposed to proceed through oxidative addition of the Cl–C bond, followed by α-chloride elimination of the Cl–R species yielding the dichlorido ruthenium carbene. However, Ru^{II} complexes are known to undergo halide atom transfer reactions with organohalides (e.g. catalyzing the Kharash reaction)[14] and thus a radical reaction between complex **3** or **4** and organohalides could not be excluded. Given our interest in the chemistry of metalloradicals and metallocarbenes,[10,15] we decided to investigate the reaction of the low-valent Ru^{I} and Ru^0 complexes with dichloromethane.

Dissolving **4** in dichloromethane resulted in the formation of **2** as evidenced by in situ ^{31}P NMR spectroscopy (see the Supporting Information). As no other complexes were detected in the ^{31}P NMR spectrum, the formation of a metallocarbene intermediate seemed unlikely. We hypothesized that the formation of **2** from **4** could proceed via a radical mechanism in which two chlorine atoms are stepwise abstracted from dichloromethane by the ruthenium complex, leading to two sequential one-electron oxidations of the metal center. This would imply that the Ru^{I} complex **3** should be an intermediate. To test this hypothesis, we added two drops of CH_2Cl_2 to a solution of **3** in [d$_8$]THF. This brown solution turned into a light-brown-colored suspension within 3 days and ^{31}P NMR spectroscopy indicated clean formation of **2**. No signals corresponding to residual **3** were observed by EPR spectroscopy, which indeed shows that **3** can undergo one-electron oxidation through chlorine atom transfer from dichloromethane. Complex **2** is stable in CH_2Cl_2 or $CHCl_3$. Having established that **2** can be formed by chlorine atom transfer to **3**, we investigated whether complex **3** can be formed from **4** by the same type of transformation. When 1 molar equivalent of CH_2Cl_2 was added to an in situ-generated solution of **4** in THF a strong EPR signal characteristic for formation of **3** was observed after 20 h. This observation indeed points to radical-type reactivity of the closed-shell Ru^0 complex **4**.

In conclusion, although the formation of Ru^{I} and Ru^0 compounds is rare, we found that the tripodal tetraphosphine scaffold **1** can accommodate ruthenium metal center in the oxidation states Ru^{II}, Ru^{I}, and Ru^0. These complexes are sufficiently stable to be isolated and analyzed by X-ray analysis. Initial reactivity studies show that both open-shell Ru^{I} and closed-shell Ru^0 complexes can undergo facile (net) abstraction of a Cl·atom from dichloromethane, resulting in the formation of the corresponding Ru^{II} and Ru^{I} complexes **2** and **3**. These results show that indole-based tetraphosphorus ligands provide a useful scaffold to explore the chemistry of low-valent ruthenium species. Future studies should aim at application of these systems in catalytic atom transfer reactions.

Acknowledgements

We thank the National Research School Combination Catalysis (NRSC-C) and the Netherlands Organization for Scientific Research (NWO-CW, VENI grant 722.013.002 for W.I.D.) and the University of Amsterdam (RPA Sustainable Chemistry) for funding. We thank Jan Meine Ernsting for assistance with NMR spectroscopy, Ed Zuidinga for mass spectrometry and Monalisa Goswami for assistance with EPR spectroscopy measurements.

Conflict of interest

The authors declare no conflict of interest.

Keywords: chloride atom abstraction · dinitrogen complexes · metalloradicals · ruthenium · tripodal ligands

[1] a) R. Poli, *Angew. Chem. Int. Ed.* **2011**, *50*, 43–45; *Angew. Chem.* **2011**, *123*, 43–45; b) M. C. Baird, *Chem. Rev.* **1988**, *88*, 1217–1227; c) K. K. Pandey, *Coord. Chem. Rev.* **1992**, *121*, 1–42; d) B. De Bruin, D. G. H. Hetterscheid, A. J. J. Koekkoek, H. Grützmacher in *Prog. Inorg. Chem. Vol. 55* (Ed.: K. D. Karlin), John Wiley & Sons, Inc., Hoboken, NJ, **2007**, pp. 252–258.
[2] a) G. Zotti, G. Pilloni, M. Bressan, M. Martelli, *J. Electroanal. Chem.* **1977**, *75*, 607–612; b) S. D. Robinson, M. F. Uttley, *J. Chem. Soc. Dalton Trans.* **1972**, 1–5; c) R. Gilbert-Wilson, L. D. Field, S. B. Colbran, M. M. Bhadbhade, *Inorg. Chem.* **2013**, *52*, 3043–3053; d) D. Davalian, P. J. Garratt, M. M. Mansuri, *J. Am. Chem. Soc.* **1978**, *100*, 980–981; e) C. Bianchini, M. Peuzzini, A. Ceccanti, F. Laschi, P. Zanello, *Inorg. Chim. Acta* **1997**, *259*, 61–70; f) R. J. Angelici, B. Zhu, S. Fedi, F. Laschi, P. Zanello, *Inorg. Chem.* **2007**, *46*, 10901–10906.
[3] A. Takaoka, L. C. H. Gerber, J. C. Peters, *Angew. Chem. Int. Ed.* **2010**, *49*, 4088–4091; *Angew. Chem.* **2010**, *122*, 4182–4185.
[4] A. Takaoka, M. E. Moret, J. C. Peters, *J. Am. Chem. Soc.* **2012**, *134*, 6695–6706.
[5] X. Yang, T. L. Gianetti, J. Harbort, M. D. Wörle, L. Tan, C.-Y. Su, P. Jurt, J. R. Harmer, H. Grützmacher, *Angew. Chem. Int. Ed.* **2016**, *55*, 11999–12002; *Angew. Chem.* **2016**, *128*, 12178–12181.
[6] a) J. Wassenaar, B. de Bruin, M. A. Siegler, A. L. Spek, J. N. H. Reek, J. I. van der Vlugt, *Chem. Commun.* **2010**, *46*, 1232–1234; b) J. Wassenaar, M. A. Siegler, A. L. Spek, B. De Bruin, J. N. H. Reek, J. I. van der Vlugt, *Inorg. Chem.* **2010**, *49*, 6495–6508. For bidentate analogues of this ligand, see: c) J. Wassenaar, J. N. H. Reek, *Dalton Trans.* **2007**, 3750–3753; d) J. Wassenaar, M. Kuil, J. N. H. Reek, *Adv. Synth. Catal.* **2008**, *350*, 1610–1614; e) J. Wassenaar, S. van Zutphen, G. Mora, P. Le Floch, M. A. Siegler, A. L. Spek, J. N. H. Reek, *Organometallics* **2009**, *28*, 2724–2734; f) J. Wassenaar, J. N. H. Reek, *J. of Org. Chem* **2009**, *74*, 8403–8406.
[7] D. Pennon, I. O. Koshevoy, F. Estevan, M. Sanaú, M. A. Ubeda, J. Pérez-Prieto, *Organometallics* **2010**, *29*, 703–706.
[8] a) L. D. Field, R. W. Guest, K. Q. Vuong, S. J. Dalgarno, P. Jensen, *Inorg. Chem.* **2009**, *48*, 2246–2253; b) G. Jia, S. D. Drouin, P. G. Jessop, A. J. Lough, R. H. Morris, *Organometallics* **1993**, *12*, 906–916.
[9] B. Jana, A. Ellern, O. Pestovsky, A. Sadow, A. Bakac, *Inorg. Chem.* **2011**, *50*, 3010–3016.
[10] a) B. de Bruin, T. P. J. Peters, S. Thewissen, A. N. J. Blok, J. B. M. Wilting, R. de Gelder, J. M. M. Smits, W. Gal, *Angew. Chem. Int. Ed.* **2002**, *41*, 2135–2138; *Angew. Chem.* **2002**, *114*, 2239–2242; b) D. G. H. Hetterscheid, J. Kaiser, E. Reijerse, T. P. J. Peters, S. Thewissen, A. N. J. Blok, J. M. M. Smits, R. de Gelder, B. de Bruin, *J. Am. Chem. Soc.* **2005**, *127*, 1895–1905; c) D. G. H. Hetterscheid, B. de Bruin, J. M. M. Smits, A. W. Gal, *Organometallics* **2003**, *22*, 3022–3024; d) D. G. H. Hetterscheid, M. Klop, R. J. N. A. M. Kicken, J. M. M. Smits, E. J. Reijerse, B. de Bruin, *Chem. Eur. J.* **2007**, *13*, 3386–3405; e) D. G. H. Hetterscheid, M. Bens, B. de Bruin, *Dalton Trans.* **2005**, 979–984.
[11] A. W. Addison, T. N. Rao, J. Reedijk, J. van Rijn, G. C. Verschoor, *J. Chem. Soc. Dalton Trans.* **1984**, 1349–1356.
[12] P. L. Holland, *Dalton Trans.* **2010**, *39*, 5415–5425.
[13] a) W. R. Roper, *J. Organomet. Chem.* **1986**, *300*, 167–190; b) T. R. Belderrain, R. H. Grubbs, *Organometallics* **1997**, *16*, 4001–4003.
[14] a) M. S. Kharasch, E. V. Jensen, W. H. Urry, *Science* **1945**, *102*, 128; b) R. P. Nair, T. H. Kim, B. J. Frost, *Organometallics* **2009**, *28*, 4681–4688.
[15] a) W. I. Dzik, J. N. H. Reek, B. De Bruin, *Chem. Eur. J.* **2008**, *14*, 7594–7599; b) W. I. Dzik, X. Xu, X. P. Zhang, J. N. H. Reek, B. de Bruin, *J. Am. Chem. Soc.* **2010**, *132*, 10891–10902; c) H. Lu, W. I. Dzik, X. Xu, L. Wojtas, B. de Bruin, X. P. Zhang, *J. Am. Chem. Soc.* **2011**, *133*, 8518–8521; d) N. D. Paul, A. Chirila, H. Lu, X. P. Zhang, B. de Bruin, *Chem. Eur. J.* **2013**, *19*, 12953–12958; e) N. D. Paul, S. Mandal, M. Otte, X. Cui, X. P. Zhang, B. de Bruin, *J. Am. Chem. Soc.* **2014**, *136*, 1090–1096; f) Y. W. Chan, B. de Bruin, K. S. Chan, *Organometallics* **2015**, *34*, 2849–2857; g) T. J. Korstanje, J. I. van der Vlugt, C. J. Elsevier, B. de Bruin, *Science* **2015**, *350*, 298–302; h) M. Goswami, C. Rebreyend, B. de Bruin, *Molecules* **2016**, *21*, 242–257; i) B. G. Das, A. Chirila, M. Tromp, J. N. H. Reek, B. de Bruin, *J. Am. Chem. Soc.* **2016**, *138*, 8968–8975; j) A. Chirila, B. G. Das, N. D. Paul, B. de Bruin, *ChemCatChem* **2017**, *9*, 1413–1421; k) M. Goswami, B. de Bruin, W. I. Dzik, *Chem. Commun.* **2017**, *53*, 4382–4385.
[16] CCDC 1555408 (**2**), 1555409 (**3**), and 1555410 (**4**) contain the supplementary crystallographic data for this paper. These data can be obtained free of charge from The Cambridge Crystallographic Data Centre.

Manuscript received: June 13, 2017
Revised manuscript received: July 28, 2017
Accepted manuscript online: August 16, 2017
Version of record online: August 30, 2017

